IEEE Photonics Journal
An IEEE Photonics Society Publication

Open Access

Photonic Image Rejection Mixer Based on Polarization Manipulation of a Broadband Optical Source

Volume 13, Number 2, April 2021

Zhiyao Jia
Guangyi Li
Difei Shi
Ming Li
Ning Hua Zhu
Wei Li

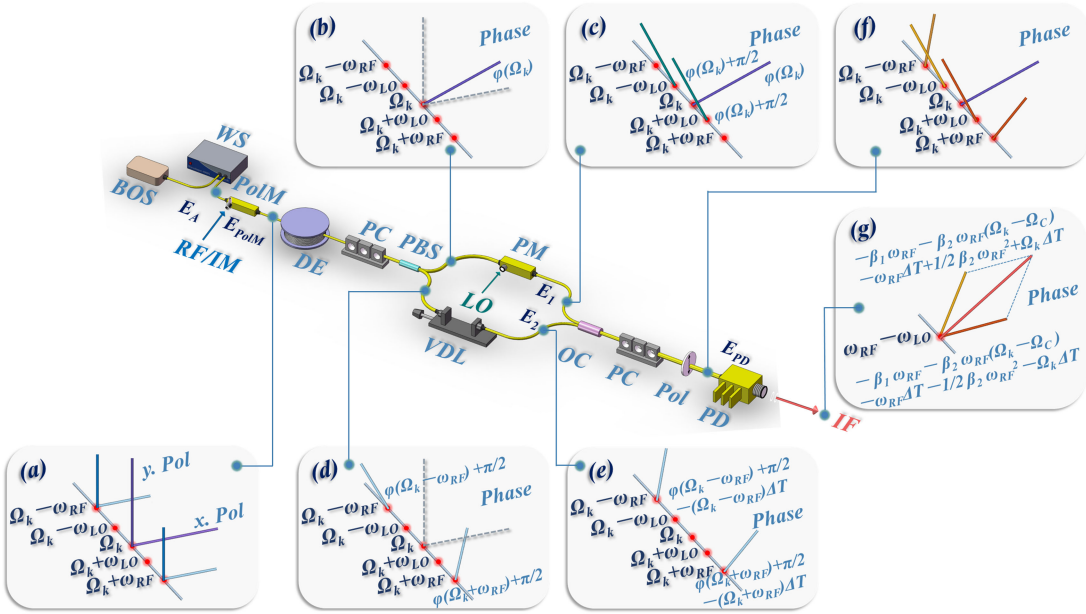

DOI: 10.1109/JPHOT.2021.3065216

Photonic Image Rejection Mixer Based on Polarization Manipulation of a Broadband Optical Source

Zhiyao Jia,[1,2,3] **Guangyi Li**,[1,2,3] **Difei Shi**,[1,2,3] **Ming Li**,[1,2,3] **Ning Hua Zhu**,[1,2,3] **and Wei Li**[1,2,3]

[1]State Key Laboratory on Integrated Optoelectronics, Institute of Semiconductors, Chinese Academy of Sciences, Beijing 100083, China
[2]School of Electronic, Electrical and Communication Engineering, University of Chinese Academy of Sciences, Beijing 100049, China
[3]Center of Materials Science and Optoelectronics Engineering, University of Chinese Academy of Sciences, Beijing 100190, China

DOI:10.1109/JPHOT.2021.3065216

Manuscript received January 23, 2021; revised March 1, 2021; accepted March 5, 2021. Date of publication March 11, 2021; date of current version March 26, 2021. This work was supported in part by the National Natural Science Foundation of China under Grants 61835010 and 60620106013 and in part by the National Key Research and Development Program of China under Grant 2019YFB2203201.
Corresponding author: Wei Li (e-mail: liwei05@semi.ac.cn).

Abstract: We propose a photonic mixer with image rejection capability using a broadband optical source (BOS) and polarization processing. Intermediate frequency (IF) signals with image rejection are generated from the local oscillator-modulated and the time-delayed radio frequency (RF)-modulated BOS light. The RF operating frequency is flexibly tunable over a wide range by simply adjusting the time delay. In addition, the proposed system is free from dispersion-induced mixing power fading and bias drift problem. Experimental results exhibit an image rejection ratio of more than 44.6 dB for RF signals from 2 to 18 GHz, while the IF signal is fixed at 800 MHz. Image rejection mixing operation at different IF frequencies and signal power is also confirmed.

Index Terms: Microwave photonics, image rejection, broadband optical source, polarization manipulation.

1. Introduction

Frequency down-conversion of radio frequency (RF) signals is of critical importance for signal processing in microwave systems such as electronic warfare, wireless communication and radar [1]–[3]. Photonic microwave mixers have attracted increasing attention in recent years for its low loss, flexible tunability, electromagnetic interference immunity and compatibility with radio-over-fiber systems [4]–[6]. However, the image interference and the desired RF signal, which are located symmetrically with respect to the local oscillator (LO) signal, are down-converted to the identical intermediate frequency (IF) band, thus a deteriorated IF signal is generated and the performance of the system is degraded.

The first well-known approach to accomplishing image rejection mixing is the phase-cancellation technology based on Hartley architecture, where parallel quadrature IF signals are combined via a 90° electrical hybrid, thus the two IF components originated from the image are out of phase and can be suppressed [7]–[19]. Quadrature IF signals can be acquired through a pair of quadrature

RF [8] or LO [9] signals generated from an electrical hybrid. The image rejection performance of these schemes depends on the electrical hybrid, which means an electrical hybrid with a precise 90° phase difference over a wide frequency range is required. In [10]–[12], a 90° optical hybrid has been introduced to generate quadrature LO-modulated sidebands, which faces the same challenge as the case of using electrical hybrids. A promising method for precise phase shift is to construct a microwave photonic phase shifter based on single sideband (SSB) modulation [13]–[19]. Unfortunately, the systems employing optical filters to select the desired sidebands [13]–[18] are sensitive to the wavelength fluctuation of the optical carrier and suffer from the constrained RF operating range. Recently, filter-free image rejection mixing has been successfully realized by the joint use of a polarization division multiplexing dual-parallel Mach-Zehnder modulator and three electrical hybrids [19]. However, sophisticated controls of bias voltages are required for carrier-suppressed SSB modulation. In addition, the phase cancellation-based schemes are sensitive to the imbalances of length and amplitude between parallel signal paths.

Another method of realizing image rejection mixing is pre-filtering the image from RF signals. For instance, the image component has been rejected by an electrical bandpass filter in [20], where multiple-stage frequency conversion has been utilized to realize a wide RF operating range, yet at the expense of a complex structure. A Fabry–Perot filter has been employed to accurately remove the image-modulated sidebands without affecting the RF-modulated sidebands [21], which may not be suitable for relatively low IF band due to the limited roll-off factor of the optical filter. In this context, stimulated Brillouin scattering (SBS) gain and loss spectrum with wide tunability and narrow bandwidth has been utilized in photonic mixing operation to process optical sidebands induced by RF or LO signals [22]–[24]. IF signals at hundreds of megahertz were successfully acquired with effective image suppression as expected. Nevertheless, an extra wideband microwave source is indispensable to generation of pump signals, which increases the complexity and cost of the SBS-based schemes.

In this paper, we propose a photonic microwave image rejection mixer (IRM) based on polarization manipulation of a broadband optical source (BOS). Thanks to the frequency selectivity provided by tunable time delay and non-coherent property of the BOS light [25], the desired RF signals are down-converted with image suppression through properly adjusting the time delay difference between the RF- and the LO-modulated signals. It is noted that most of previous laser-based photonic image rejection schemes require SSB modulation, which is implemented by optical filters or electrical hybrids in conjunction with complicated bias control [10]–[19]. In our work, SSB modulation is no more necessary, which ensures a comparatively convenient operation and a wide operating frequency range. Moreover, power fading of mixing outputs, which normally exists under circumstance of the combination of chromatic dispersion and double sideband modulation [26], is removed in our scheme. A proof-of-concept experiment confirms an effective image suppression across a wide frequency range.

2. Principle

The proposed IRM is schematically illustrated in Fig. 1. The spectrally shaped BOS light is polarization modulated by the RF signal and sent to a polarization beam splitter (PBS) through a dispersive element (DE). The modulated signal is polarization demultiplexed into two branches by the PBS, where the upper one is phase-modulated by the LO signal, and the lower one is time delayed. The two branches are subsequently coupled together with the same polarization, and the IF signal with image suppression can be acquired after photodetection.

The BOS light consists of continuously distributed frequency components which are incoherent to each other. The shaped signal in frequency domain can be described as a stochastic process $E_A(\Omega)$, whose statistical property is mathematically given by [25]

$$\left\langle E_A(\Omega) E_A^*(\Omega') \right\rangle = 2\pi N(\Omega) \delta(\Omega - \Omega'), \tag{1}$$

where Ω is the angular frequency and $N(\Omega)$ is the power spectral density of the BOS light.

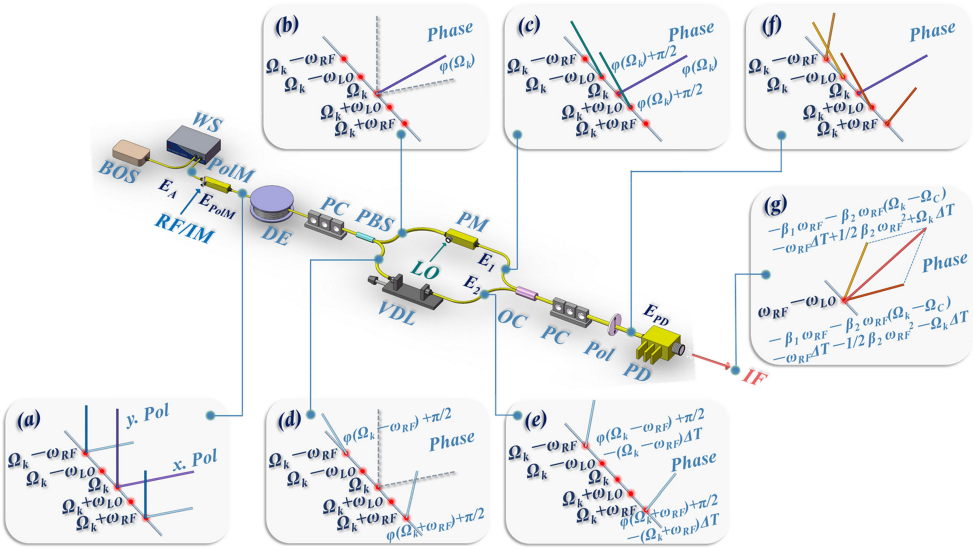

Fig. 1. Schematic diagram of the proposed IRM. BOS: broadband optical source, WS: waveshaper, PolM: polarization modulator, DE: dispersive element, PC: polarization controller, PBS: polarization beam splitter, PM: phase modulator, VDL: variable delay line, OC: optical coupler, Pol: polarizer, PD: photodetector, RF: radio frequency, IM: image, LO: local oscillator, IF: intermediate frequency. (a)-(g) Principle illustration by spectrum evolution of the optical and electrical signals generated from a single frequency component of the BOS.

A polarization modulator (PolM) is utilized to achieve phase modulation with opposite modulation indices at the two orthogonal principal axes. A polarizer is integrated at front of the PolM, and aligned at 45° to its principal axes. Thus, the BOS signal after polarization modulation can be expressed as

$$E_{\mathrm{PolM}}(\Omega)=\begin{bmatrix}E_{\mathrm{x}}(\Omega)\\ E_{\mathrm{y}}(\Omega)\end{bmatrix}=\frac{\sqrt{2}}{2}\begin{bmatrix}\frac{1}{2\pi}E_{\mathrm{A}}(\Omega)\otimes\mathcal{F}\left[\exp\left(jm_{\mathrm{RF}}\cos\omega_{\mathrm{RF}}t\right)\right]\\ \frac{1}{2\pi}E_{\mathrm{A}}(\Omega)\otimes\mathcal{F}\left[\exp\left(-jm_{\mathrm{RF}}\cos\omega_{\mathrm{RF}}t\right)\right]\end{bmatrix}$$
$$=\frac{\sqrt{2}}{2}\begin{bmatrix}\sum_{k=-\infty}^{+\infty}j^{k}J_{k}(m_{\mathrm{RF}})E_{\mathrm{A}}(\Omega-k\omega_{\mathrm{RF}})\\ \sum_{k=-\infty}^{+\infty}(-j)^{k}J_{k}(m_{\mathrm{RF}})E_{\mathrm{A}}(\Omega-k\omega_{\mathrm{RF}})\end{bmatrix},\tag{2}$$

where $\otimes$ and $\mathcal{F}[\cdot]$ are convolution and Fourier transform operators, respectively. ω_{RF} is the angular frequency of the RF signal to be down-converted. $m_{\mathrm{RF}}=\pi V_{\mathrm{RF}}/V\pi$ is the modulation index of the PolM, where V_{RF} and V_{π} are the amplitude of the driven RF signal and the half-wave voltage of the modulator, respectively. Jacob-Anger expansion is also applied, and $J_{\mathrm{k}}(m_{\mathrm{RF}})$ is the Bessel function of the first kind of order k. It is noted that even-order sidebands including optical carrier and odd-order sidebands can be respectively generated at two orthogonal polarization states, which show ±45° off relative to the x axis of the PolM. The polarization-multiplexed optical signal can be expressed as

$$E_{\mathrm{PolM}}(\Omega)=\begin{bmatrix}E_{\mathrm{x}+45^{\circ}}(\Omega)\\ E_{\mathrm{x}-45^{\circ}}(\Omega)\end{bmatrix}=\begin{bmatrix}\frac{\sqrt{2}}{2}E_{\mathrm{x}}(\Omega)+\frac{\sqrt{2}}{2}E_{\mathrm{y}}(\Omega)\\ \frac{\sqrt{2}}{2}E_{\mathrm{x}}(\Omega)-\frac{\sqrt{2}}{2}E_{\mathrm{y}}(\Omega)\end{bmatrix}$$
$$=\begin{bmatrix}\sum_{q=-\infty}^{+\infty}(-1)^{q}J_{2q}(m_{\mathrm{RF}})E_{\mathrm{A}}(\Omega-2q\omega_{\mathrm{RF}})\\ \sum_{n=-\infty}^{+\infty}(-1)^{n}jJ_{2n+1}(m_{\mathrm{RF}})E_{\mathrm{A}}[\Omega-(2n+1)\omega_{\mathrm{RF}}]\end{bmatrix}.\tag{3}$$

The modulated signal is fed to the DE characterized by a group time delay of β_1 and a total dispersion of β_2. Its transmission function is given by Taylor expansion as

$$H_{\mathrm{DE}}(\Omega) = \mathrm{e}^{-j\left[\beta_0+\beta_1(\Omega-\Omega_{\mathrm{C}})+\frac{\beta_2}{2}(\Omega-\Omega_{\mathrm{C}})^2\right]}, \tag{4}$$

where β_0 is a constant and Ω_{C} is the central angular frequency of the shaped spectrum. The two polarization states are aligned with two principal axes of the PBS by adjusting the polarization controller (PC), and thus odd-order and even-order sidebands are separately acquired at two outputs of the PBS. A phase modulator (PM) is located at the upper branch to allow the even-order sidebands to be modulated by the LO signal, while a variable delay line (VDL) is utilized to introduce a tunable time delay ΔT to the odd-order sidebands at the lower branch. The LO-modulated signal and the time-delayed signal are respectively given by

$$\begin{aligned} E_1(\Omega) &= \frac{1}{2\pi} E_{\mathrm{x}+45^\circ}(\Omega) H_{\mathrm{DE}}(\Omega) \otimes \mathcal{F}\left[\exp\left(jm_{\mathrm{LO}}\cos\omega_{\mathrm{LO}}t\right)\right] \\ &= \sum_{q=-\infty}^{+\infty}\sum_{l=-\infty}^{+\infty} (-1)^q j^l J_{2q}(m_{\mathrm{RF}}) J_l(m_{\mathrm{LO}}) E_{\mathrm{A}}(\Omega - 2q\omega_{\mathrm{RF}} - l\omega_{\mathrm{LO}}) H_{\mathrm{DE}}(\Omega - l\omega_{\mathrm{LO}}), \end{aligned} \tag{5}$$

$$\begin{aligned} E_2(\Omega) &= E_{\mathrm{x}-45^\circ}(\Omega) H_{\mathrm{DE}}(\Omega) \exp(-j\Omega\Delta T) \\ &= \sum_{n=-\infty}^{+\infty} (-1)^n j J_{2n+1}(m_{\mathrm{RF}}) E_{\mathrm{A}}[\Omega - (2n+1)\omega_{\mathrm{RF}}] H_{\mathrm{DE}}(\Omega) \exp(-j\Omega\Delta T). \end{aligned} \tag{6}$$

Similar to (2), ω_{LO} and $\mathrm{m_{LO}}$ are the angular frequency of the LO signal and modulation index of the PM, respectively. With the assistance of an optical coupler, a PC and a polarizer, the two optical signals are recombined together at the same polarization. Under small signal modulation, the signal injected into the photodetector (PD) is expressed by

$$\begin{aligned} E_{\mathrm{PD}}(\Omega) &= \frac{\sqrt{2}}{2} E_1(\Omega) + \frac{\sqrt{2}}{2} E_2(\Omega) \\ &= \frac{\sqrt{2}}{2} J_0(m_{\mathrm{RF}}) J_0(m_{\mathrm{LO}}) E_{\mathrm{A}}(\Omega) H_{\mathrm{DE}}(\Omega) + \frac{\sqrt{2}}{2} j J_0(m_{\mathrm{RF}}) J_1(m_{\mathrm{LO}}) E_{\mathrm{A}}(\Omega - \omega_{\mathrm{LO}}) H_{\mathrm{DE}}(\Omega - \omega_{\mathrm{LO}}) \\ &+ \frac{\sqrt{2}}{2} j J_0(m_{\mathrm{RF}}) J_1(m_{\mathrm{LO}}) E_{\mathrm{A}}(\Omega + \omega_{\mathrm{LO}}) H_{\mathrm{DE}}(\Omega + \omega_{\mathrm{LO}}) + \frac{\sqrt{2}}{2} j J_1(m_{\mathrm{RF}}) E_{\mathrm{A}}(\Omega - \omega_{\mathrm{RF}}) H_{\mathrm{DE}}(\Omega) \exp(-j\Omega\Delta T) \\ &+ \frac{\sqrt{2}}{2} j J_1(m_{\mathrm{RF}}) E_{\mathrm{A}}(\Omega + \omega_{\mathrm{RF}}) H_{\mathrm{DE}}(\Omega) \exp(-j\Omega\Delta T). \end{aligned} \tag{7}$$

Accordingly, the generated IF signal after photodetection can be given by

$$i_{\mathrm{RF}}(\omega_{\mathrm{IF}}) = \frac{\gamma}{2\pi}\left\langle \int_0^{\infty} E_{\mathrm{PD}}(\Omega) E_{\mathrm{PD}}^{*}(\Omega - \omega_{\mathrm{IF}})\, d\Omega \right\rangle, \tag{8}$$

where γ denotes the influence of the link loss and the responsivity of the PD. As can be seen from (1) and (8), the generated IF signal is the accumulation of beats between the RF- and LO-modulated sidebands originated from the identical frequency component of the BOS due to its incoherent characteristic. Spectra of the optical sidebands and IF signals corresponding to a single frequency component Ω_{k} are schematically shown in Figs. 1(a)-1(g), where $\varphi(\cdot)$ denotes the phase shift induced by the DE.

Therefore, the IF signal down-converted from the desired RF signal can be given by

$$\begin{aligned} i_{\mathrm{RF}}(\omega_{\mathrm{IF}}) &= \frac{\gamma}{2} J_1(m_{\mathrm{RF}}) J_1(m_{\mathrm{LO}}) J_0(m_{\mathrm{RF}}) \exp\left[-j\left(\beta_1\omega_{\mathrm{RF}} - \frac{1}{2}\beta_2\omega_{\mathrm{RF}}^2 - \Omega_{\mathrm{C}}\Delta T + \omega_{\mathrm{RF}}\Delta T\right)\right] \\ &\quad H_{\mathrm{b}}\left(\omega_{\mathrm{RF}} - \frac{\Delta T}{\beta_2}\right), \end{aligned} \tag{9}$$

where $H_b(\omega)$ is a baseband response given by

$$H_b(\omega) = \int_0^{\infty} N(\Omega) \exp\left[-j\beta_2(\Omega - \Omega_C)\omega\right] d\Omega. \tag{10}$$

For the image with an angular frequency of ω_{IM}, the mathematical deduction is similar to the case of the RF signal illustrated in (2)–(8). The IF signal generated from the image is given as follows

$$i_{IM}(\omega_{IF}) = \frac{\gamma}{2} J_1(m_{IM}) J_1(m_{LO}) J_0(m_{IM}) \exp\left[j\left(\beta_1\omega_{IM} - \frac{1}{2}\beta_2\omega_{IM}^2 - \Omega_C\Delta T + \omega_{IM}\Delta T\right)\right] H_b^*\left(\omega_{IM} - \frac{\Delta T}{\beta_2}\right). \tag{11}$$

As can be seen from (9) and (11), a bandpass filter centered at $\Delta T/\beta_2$ is equivalently constructed at the front of the system. The inherent filtering characteristic can be attributed to the continuous impulse response, which is provided by continuously distributed frequency components of the BOS light with different complex coefficients given by dispersion.

The image rejection ratio (IRR), which is defined as the power ratio between the IF signal down-converted from the RF signal and from the image, is given by $|H_b(\omega_{RF} - \Delta T/\beta_2)/H_b(\omega_{IM} - \Delta T/\beta_2)|^2$. It indicates that the IRR in the proposed scheme depends on the suppression effect of the filter response on the RF signal and the image. Fortunately, a tunable filter with narrow bandwidth can be realized by adjusting the waveshaper (WS) since the filter characterize a proportional version of the Fourier transformation of the shaped BOS light, which is indicated by (10). Consequently, the image can be successfully suppressed even for the comparatively low IF. Furthermore, RF signals with different frequencies can be conveniently down-converted with image suppression by adjusting the VDL.

It is worth noting that in (9), the dispersion-induced phase shift (i.e., $\varphi_{dis} = 1/2\beta_2\omega_{RF}^2$) manipulates the phase rather than amplitude of the IF signal, which indicates that the power fading resulted from double sideband modulation and chromatic dispersion is avoided. It can be further illustrated by the electrical spectra shown in Fig. 1(g). The phase difference between the two IF signals, which are respectively originated from the two upper sidebands and the two lower sidebands, is determined by the frequency dependent phase shift induced by time delay (i.e., $\Omega_k\Delta T$) besides φ_{dis}. As a consequent, the amplitude of the interference signal between the two IF photocurrents varies periodically versus the optical carrier frequency, and φ_{dis} eventually makes no influence on the IF amplitude after accumulation among those frequency components.

3. Experiments and Results

A proof-of-concept experiment based on the configuration shown in Fig. 1 was carried out to verify the feasibility of the proposed image-reject mixer. A BOS light provided by an amplified spontaneous emission light source (Lightcomm) was filtered by a WS (Finisar 4000S), which was programmed as a Gaussian filter with a center wavelength of 1555 nm and a full width at half maximum (FWHM) of 8 nm. The shaped BOS light measured by an optical spectrum analyzer (YOKOGAWA AQ6370D) is shown in Fig. 2(a). After compensation for the insertion loss of the WS by an erbium-doped fiber amplifier (EDFA, KEOPSYS), the BOS light was coupled to a PolM (Versawave), which was driven by the RF signal or image generated by a vector network analyzer (VNA, Rohde & Schwarz ZVA40). The DE used in the experiment was a 5 km dispersion compensating fiber with a total dispersion of -803 ps/nm. A PM (EOSpace) driven by a LO signal from an analog signal generator (Keysight N5183B) was located at the upper branch, while a tunable optical delay line (TODL, OZ Optics Ltd) with 330 ps tunable range was placed at the lower branch. A PD (Agilent 11982A) was utilized to convert the polarized signal after another EDFA (JDS Uniphase). The generated IF signal was boosted by an electrical amplifier (EA, SHF) with a gain of 11.5 dB, and subsequently measured by a spectrum analyzer (Rohde & Schwarz).

Firstly, the RF signal was fixed at 6 GHz with a power of 5 dBm to demonstrate the performance of image suppression. A bandpass filter (i.e., $H_b(\omega - \Delta T/\beta_2)$) centered at 6 GHz was realized by adjusting the TODL. Fig. 2(b) shows the transfer function of the filter measured by the VNA.

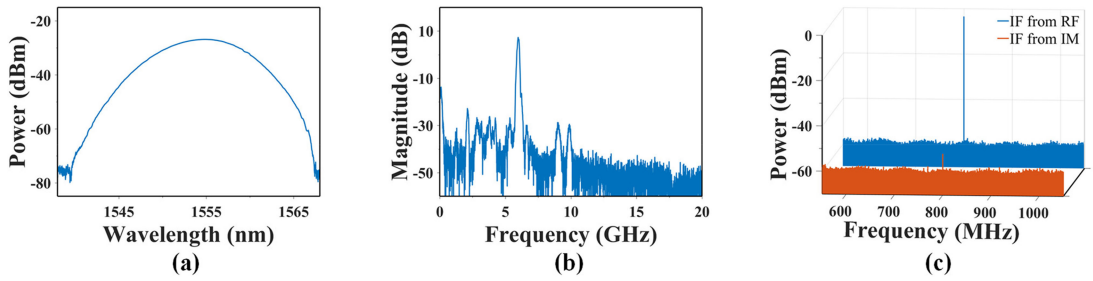

Fig. 2. Measured (a) optical spectrum of the shaped BOS light, (b) magnitude response of the bandpass filter and (c) electrical spectra of the IF signals.

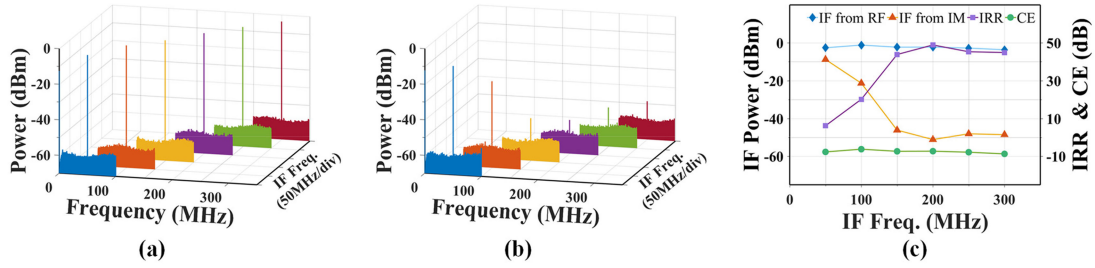

Fig. 3. Measured IF signals with frequencies from 50 to 300 MHz. Electrical spectra of the IF signals down-converted from (a) the RF signals and (b) the image. (c) The corresponding IF signal power, IRR and CE.

It is characterized by a Gaussian profile with a 3-dB bandwidth of 131 MHz, which agrees well with the theoretical analysis. It is noted that the 3-dB bandwidth of the bandpass filter limits the instantaneous bandwidth of the proposed IRM, which may not be suitable for processing broadband RF signals. Though the instantaneous bandwidth can be improved through reducing the FWHM of the Gaussian filter provided by the WS, a microwave photonic bandpass filter with broaden bandwidth may lead to a worsen IRR. Therefore, the bandwidth of the shaped BOS light should be carefully selected to make the instantaneous bandwidth and the IRR appropriate for specific applications. A LO signal with a frequency of 5.2 GHz and a power of 5 dBm was fed to the PM for frequency down-conversion. The 800 MHz IF signal with a power of -3.4 dBm was generated accordingly, whose spectrum is shown in Fig. 2(c). The conversion efficiency (CE), which is defined as the power ratio between the IF signal and the RF signal, is calculated to be -8.4 dB. The signal from the VNA was subsequently switched to 4.4 GHz to serve as the image. The corresponding IF signal shown in Fig. 2(c) is suppressed to be 48.3 dB lower than the desired one, which confirms the image rejection mixing operation.

As discussed in the theoretical part, the IRR is dependent on the suppression effect of the filter function on the image, which means the IRR may be influenced by the frequency of the IF signal. Thus the variation of the IRR versus the IF signal was experimentally investigated. The IF signal was swept from 50 to 300 MHz with a step of 50 MHz in sequence, and the frequencies of LO signals and image changed accordingly. The power of IF signals originated from RF signals and image, as well as the corresponding IRR, are shown in Figs. 3(a), 3(b) and 3(c), respectively. It is noted that an IRR of over 43.8 dB was achieved for frequencies ranging from 150 to 300 MHz, whereas the IF signals at 50 and 100 MHz revealed a relatively deteriorative IRR. It can be ascribed to the decreasing interval between the image and the center of the filter response, which also set the lower limit of the IF signal. To further verify the tunability of the IF, signals with frequencies from 400 to 1000 MHz and an interval of 100 MHz were generated as shown in Figs. 4(a) and 4(b),

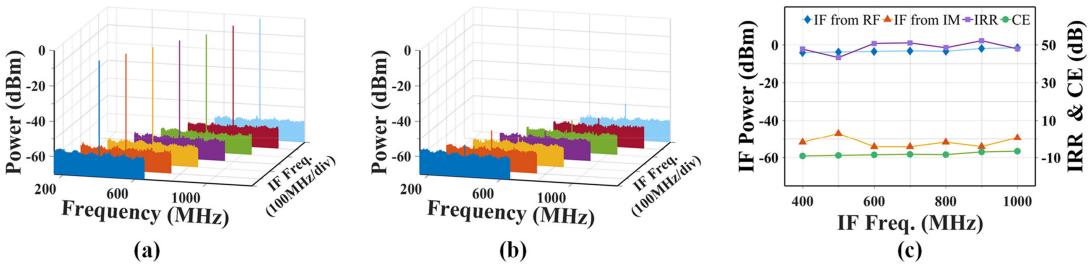

Fig. 4. Measured IF signals with frequencies from 400 to 1000 MHz. Electrical spectra of the IF signals down-converted from (a) the RF signals and (b) the image. (c) The corresponding IF signal power, IRR and CE.

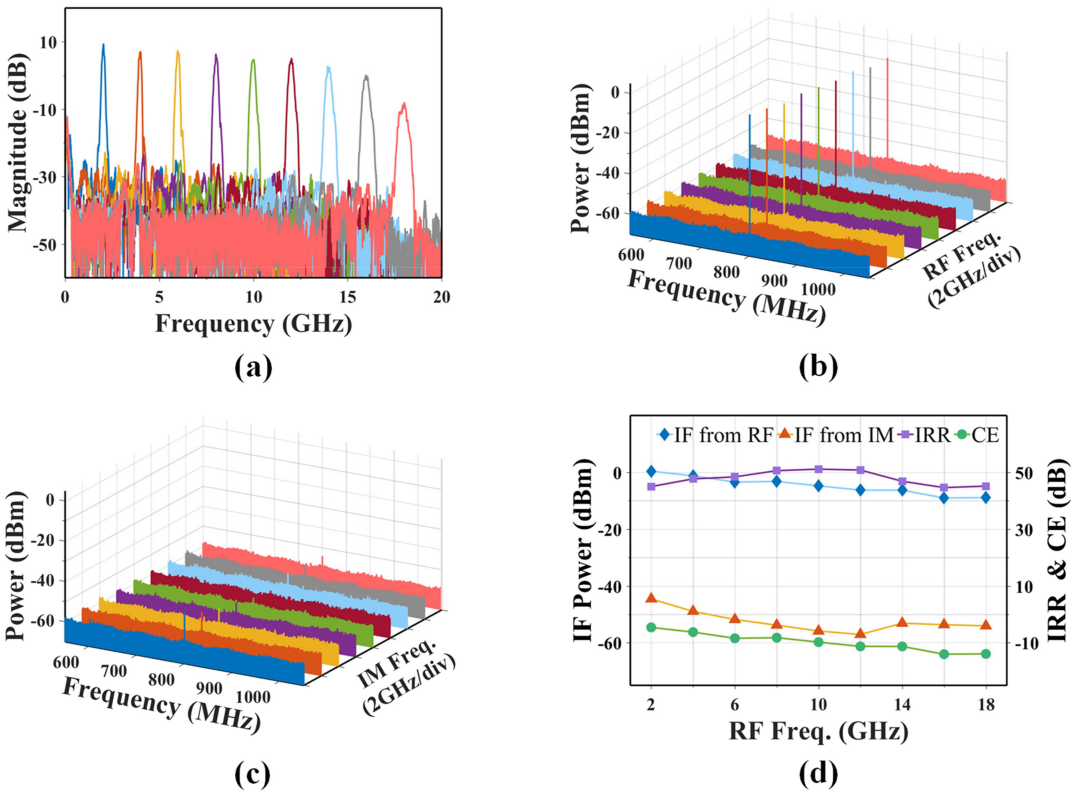

Fig. 5. Measured results with RF frequencies from 2 to 18 GHz. (a) Magnitude response of the corresponding bandpass filters. Electrical spectra of the IF signals down-converted from (b) the RF signals and (c) the image. (d) The corresponding IF signal power, IRR and CE.

which exhibits an effective suppression on the IF from image. Figs. 3(c) and 4(c) indicate that a CE of more than -9.2 dB is obtained with a slight fluctuation over the mentioned IF range.

To demonstrate that the image rejection mixing operation can be realized over a wide RF regime, the RF signal was tuned from 2 to 18 GHz with a step of 2 GHz while the IF signal was fixed at 800 MHz. As shown in Fig. 5(a), the corresponding bandpass response centered at 2-18 GHz was constructed by tunning the TODL, and an obvious decline of magnitude response is observed as the center frequency is switched to 18 GHz. The decline can be mainly attributed to the limited bandwidth of the PD utilized in our experiment. Figs. 5(b) and 5(c) show the electrical spectra of the IF signals generated from RF signals and the image, which demonstrates an IRR of more

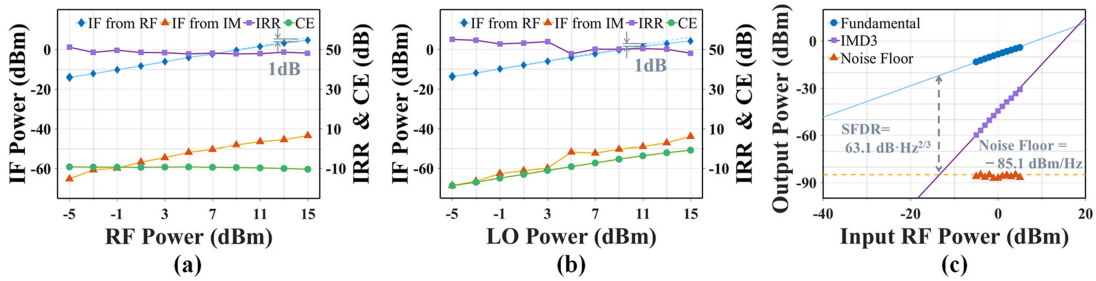

Fig. 6. Measured IF signal power, IRR and CE (a) at different RF power while the LO power is fixed at 5 dBm and (b) different LO power while the RF power is fixed at 5 dBm. (c) Measured power of the fundamental and IMD3 components versus the input RF power.

than 44.6 dB across the RF range from 2 to 18 GHz. It is noted that the CE displayed in Fig. 5(d) decreases by 9.4 dB with the RF signal varying from 2 to 18 GHz. It primarily results from the frequency dependent response of the modulators, and the bandwidth of the modulators determines the RF operating range of the proposed system. In addition, dispersion-induced power fading was eliminated for the above RF frequencies as discussed in the theoretical part.

The performance of the proposed mixer was further evaluated with respect to different signal power. The RF signal, the LO signal and the image were maintained at 6, 5.6 and 5.2 GHz, respectively. The RF power was swept from −5 to 15 dBm with an interval of 2 dB, while the LO tone was fixed at 5 dBm. As can be seen from Fig. 6(a), the power of the IF signals increases linearly with the RF power on the condition that the RF power is less than 7 dBm, and an almost constant CE with a fluctuation of about ±0.1 dB is observed. Fig. 6(a) also exhibits a 1 dB compression point of about 14.1 dBm. Fig. 6(b) shows the variation of the IF power and the CE versus LO power while the RF signal was fixed at 5 dBm. The power of the desired IF signal, as well as the CE, increases linearly with the LO power under small signal modulation, and the LO power at the 1 dB compression point is about 11.3 dBm. The IRR exhibited in Figs. 6(a) and 6(b) remains more than 47.6 dB, which illustrates that the disturbing IF components were efficiently rejected over the mentioned power range.

The higher-order RF- and LO-modulated optical sidebands are neglected in the previous theoretical derivation. To analyze the influence of the higher-order sidebands on the generated IF signal, the modulated optical sidebands up to the third-order ones are considered, in which case the optical field after the PM and the VDL can be respectively expressed as

$$\begin{aligned} E_1(\Omega) &= J_0(m_{RF})\,J_0(m_{LO})\,E_A(\Omega)\,H_{DE}(\Omega) + jJ_0(m_{RF})\,J_1(m_{LO})\,E_A(\Omega-\omega_{LO})\,H_{DE}(\Omega-\omega_{LO}) \\ &+ jJ_0(m_{RF})\,J_1(m_{LO})\,E_A(\Omega+\omega_{LO})\,H_{DE}(\Omega+\omega_{LO}) - J_0(m_{RF})\,J_2(m_{LO})\,E_A(\Omega-2\omega_{LO})\,H_{DE}(\Omega-2\omega_{LO}) \\ &- J_0(m_{RF})\,J_2(m_{LO})\,E_A(\Omega+2\omega_{LO})\,H_{DE}(\Omega+2\omega_{LO}) - jJ_0(m_{RF})\,J_3(m_{LO})\,E_A(\Omega-3\omega_{LO})\,H_{DE}(\Omega-3\omega_{LO}) \\ &- jJ_0(m_{RF})\,J_3(m_{LO})\,E_A(\Omega+3\omega_{LO})\,H_{DE}(\Omega+3\omega_{LO}) - J_0(m_{LO})\,J_2(m_{RF})\,E_A(\Omega-2\omega_{RF})\,H_{DE}(\Omega) \\ &- jJ_1(m_{LO})\,J_2(m_{RF})\,E_A(\Omega-2\omega_{RF}-\omega_{LO})\,H_{DE}(\Omega-\omega_{LO}) - jJ_1(m_{LO})\,J_2(m_{RF})\,E_A(\Omega-2\omega_{RF}+\omega_{LO}) \\ &\quad H_{DE}(\Omega+\omega_{LO}) - J_0(m_{LO})\,J_2(m_{RF})\,E_A(\Omega+2\omega_{RF})\,H_{DE}(\Omega) - jJ_1(m_{LO})\,J_2(m_{RF})\,E_A(\Omega+2\omega_{RF}-\omega_{LO}) \\ &\times H_{DE}(\Omega-\omega_{LO}) - jJ_1(m_{LO})\,J_2(m_{RF})\,E_A(\Omega+2\omega_{RF}+\omega_{LO})\,H_{DE}(\Omega+\omega_{LO}) \end{aligned} \tag{12}$$

$$\begin{aligned} E_2(\Omega) &= jJ_1(m_{RF})\,E_A(\Omega-\omega_{RF})\,H_{DE}(\Omega)\exp(-j\Omega\Delta T) + jJ_1(m_{RF})\,E_A(\Omega+\omega_{RF})\,H_{DE}(\Omega)\exp(-j\Omega\Delta T) \\ &- jJ_3(m_{RF})\,E_A(\Omega-3\omega_{RF})\,H_{DE}(\Omega)\exp(-j\Omega\Delta T) - jJ_3(m_{RF})\,E_A(\Omega+3\omega_{RF})\,H_{DE}(\Omega)\exp(-j\Omega\Delta T). \end{aligned} \tag{13}$$

The IF signals from the desired RF signal and the image interference are thus given by

$$i_{RF}(\omega_{IF}) = \frac{\gamma}{2} J_1(m_{RF}) J_1(m_{LO}) J_0(m_{RF}) \exp\left[-j\left(\beta_1\omega_{RF} - \frac{1}{2}\beta_2\omega_{RF}^2 - \Omega_C\Delta T + \omega_{RF}\Delta T\right)\right] H_b\left(\omega_{RF} - \frac{\Delta T}{\beta_2}\right)$$
$$- \frac{\gamma}{2} J_2(m_{RF}) J_1(m_{RF}) J_1(m_{LO}) \exp\left[-j\left(\beta_1\omega_{RF} + \frac{3}{2}\beta_2\omega_{RF}^2 - \Omega_C\Delta T - \omega_{RF}\Delta T\right)\right] H_b\left(\omega_{RF} - \frac{\Delta T}{\beta_2}\right)$$
$$+ \frac{\gamma}{2} J_3(m_{RF}) J_2(m_{RF}) J_1(m_{LO}) \exp\left[-j\left(\beta_1\omega_{RF} - \frac{5}{2}\beta_2\omega_{RF}^2 - \Omega_C\Delta T + 3\omega_{RF}\Delta T\right)\right] H_b\left(\omega_{RF} - \frac{\Delta T}{\beta_2}\right), \tag{14}$$

$$i_{IM}(\omega_{IF}) = \frac{\gamma}{2} J_1(m_{IM}) J_1(m_{LO}) J_0(m_{IM}) \exp\left[j\left(\beta_1\omega_{IM} - \frac{1}{2}\beta_2\omega_{IM}^2 - \Omega_C\Delta T + \omega_{IM}\Delta T\right)\right] H_b^*\left(\omega_{IM} - \frac{\Delta T}{\beta_2}\right)$$
$$- \frac{\gamma}{2} J_2(m_{IM}) J_1(m_{IM}) J_1(m_{LO}) \exp\left[j\left(\beta_1\omega_{IM} + \frac{3}{2}\beta_2\omega_{IM}^2 - \Omega_C\Delta T - \omega_{IM}\Delta T\right)\right] H_b^*\left(\omega_{IM} - \frac{\Delta T}{\beta_2}\right)$$
$$+ \frac{\gamma}{2} J_3(m_{IM}) J_2(m_{IM}) J_1(m_{LO}) \exp\left[j\left(\beta_1\omega_{IM} - \frac{5}{2}\beta_2\omega_{IM}^2 - \Omega_C\Delta T + 3\omega_{IM}\Delta T\right)\right] H_b^*\left(\omega_{IM} - \frac{\Delta T}{\beta_2}\right). \tag{15}$$

As can be seen from (14) and (15), the second- and third-order sidebands also make contribution to the generated IF signal besides the first-order ones. However, the influence of IF signals originated from the higher-order sidebands on the IF power could be neglected due to those relatively low amplitude compared with IF signals from the first-order sidebands. In addition, nonlinear sidebands result in intermodulation products in the photocurrent, among which the third-order intermodulation distortion (IMD3) components may lie in the IF band. To investigate the nonlinear distortion of the proposed mixer, a two-tone RF signal with frequencies of 6.005 and 5.995 GHz was introduced to measure the spurious free dynamic range (SFDR). The LO signal was fixed at 5.6 GHz. Fig. 6(c) shows the power of the fundamental and IMD3 components under different input RF power. The SFDR of the proposed scheme is calculated to be 63.1 dB $\cdot$ Hz$^{2/3}$ with a measured noise floor of -85.1 dBm/Hz. The sources of noise in our system mainly include the beat noise from the BOS light, thermal noise, shot noise of photocurrent and noise induced by the EA.

4. Conclusion

In conclusion, a photonic mixer with image suppression capability using a BOS has been theoretically analyzed and experimentally demonstrated. With the assistance of intrinsic frequency selectivity of the proposed system, a bias-free image rejection operation has been realized over a wide frequency range. IF signals ranging from 150 to 1000 MHz have been successfully down-converted from the 6 GHz RF signal with effective suppression on image. An IRR of more than 44.6 dB over a RF frequency range from 2 to 18 GHz has also been experimentally demonstrated for IF signals at 800 MHz. In addition, dispersion-induced power fading has been eliminated for the above RF frequencies.

References

[1] M. E. Manka, "Microwave photonics for electronic warfare applications," in *Proc. Int. Topical Meeting Microw. Photon. Jointly Held Asia–Pacific Microw. Photon. Conf.*, Sep. 2008, pp. 275–278.
[2] F. Laghezza, F. Scotti, P. Ghelfi, and A. Bogoni, "Photonics-assisted multiband RF transceiver for wireless communications," *J. Lightw. Technol.*, vol. 32, no. 16, pp. 2896–2904, Aug. 2014.
[3] F. Scotti, F. Laghezza, P. Ghelfi, and A. Bogoni, "Multi-band software-defined coherent radar based on a single photonic transceiver," *IEEE Trans. Microw. Theory Techn.,* vol. 63, no. 2, pp. 546–552, Feb. 2015.
[4] H. J. Song and J. I. Song, "Simultaneous all-optical frequency downconversion technique utilizing an SOA-MZI for WDM radio over fiber (RoF) applications," *J. Lightw. Technol.*, vol. 24, no. 8, pp. 3028–3034, Aug. 2006.

[5] E. H. W. Chan and R. A. Minasian, "Microwave photonic downconverter with high conversion efficiency," *J. Lightw. Technol.*, vol. 30, no. 23, pp. 3580–3585, Dec. 2012.
[6] Z. Tang, Y. Li, J. Yao, and S. Pan, "Photonics-based microwave frequency mixing: Methodology and applications," *Laser Photon. Rev.*, vol. 14, no. 1, 2020, Art. no. 1800350.
[7] D. Zhu and S. Pan, "Photonics-based microwave image-reject mixer," *Photonics*, vol. 5, no. 2, p. 6, Mar. 2018.
[8] J. Zhang, E. H. W. Chan, X. Wang, X. Feng, and B. Guan, "High conversion efficiency photonic microwave mixer with image rejection capability," *IEEE Photon. J.*, vol. 8, no. 4, Aug. 2016. Art. no. 3900411.
[9] D. Shan, A. Wen, W. Zhai, X. Li, W. Zhang, and Z. Tu, "Filter-free image-reject microwave photonic downconverter based on cascaded modulators," *Appl. Opt.*, vol. 58, no. 13, pp. 3432–3437, May 2019.
[10] Z. Tang and S. Pan, "Reconfigurable microwave photonic mixer with minimized path separation and large suppression of mixing spurs," *Opt. Lett.*, vol. 42, no. 1, pp. 33–36, Jan. 2017.
[11] Z. Shi, S. Zhu, M. Li, N. H. Zhu, and W. Li, "Reconfigurable microwave photonic mixer based on dual-polarization dual-parallel mach-zehnder modulator," *Opt. Commun.*, vol. 428, pp. 131–135, Jul. 2018
[12] W. Jiang, S. Zhao, Q. Tan, D. Liang, X. Li, and Y. Gao, "Wideband photonic microwave channelization and image-reject down-conversion," *Opt. Commun.*, vol. 445, pp. 41–49, 2019.
[13] P. Li, W. Pan, X. Zou, B. Lu, L. Yan, and B. Luo, "Image-free microwave photonic down-conversion approach for fiber-optic antenna remoting," *IEEE J. Quantum Electron.*, vol. 53, no. 4, Aug. 2017, Art. no. 9100208.
[14] Y. Gao, A. Wen, W. Chen, and X. Li, "All-optical, ultra-wideband microwave I/Q mixer and image-reject frequency down-converter," *Opt. Lett.*, vol. 42, no. 6, pp. 1105–1108, Mar. 2017.
[15] Y. Gao, A. Wen, W. Jiang, Y. Fan, and Y. He, "All-optical and broadband microwave fundamental/sub-harmonic I/Q downconverters," *Opt. Exp.*, vol. 26, no. 6, pp. 7336–7350, Mar. 2018.
[16] K. Xiao, X. Jin, X. Jin, X. Yu, Q. Tan, and G. Wang, "Tunable OEO-based photonic RF receiver with image frequency rejection," *Appl. Opt.*, vol. 58, no. 8, pp. 2127–2131, Mar. 2019.
[17] S. T. Lipkowitz, T. U. Horton, and T. E. Murphy, "Wideband microwave electro-optic image rejection mixer," *Opt. Lett.*, vol. 44, no. 19, pp. 4710–4713, Oct. 2019.
[18] B. Kang *et al.*, "All-optical and broadband microwave image-reject receiver based on phase modulation and I/Q balanced detection," *J. Lightw. Technol.*, vol. 38, no. 21, pp. 5962–5972, Nov. 2020.
[19] Y. Zhang *et al.*, "Broadband image-reject mixing based on a polarization-modulated dual-channel photonic microwave phase shifter," *IEEE Photon. J.*, vol. 12, no. 2, Apr. 2020, Art. no. 7800409.
[20] S. J. Strutz and K. J. Williams, "A 0.8-8.8-GHz image rejection microwave photonic downconverter," *IEEE Photon. Technol. Lett.*, vol. 12, no. 10, pp. 1376–1378, Oct. 2000.
[21] S. J. Strutz and K. J. Williams, "An 8-18-GHz all-optical microwave downconverter with channelization," *IEEE Trans. Microw. Theory Techn.*, vol. 49, no. 10, pp. 1992–1995, Oct. 2001.
[22] X. Kong, Y. Yu, H. Tang, and X. Zhang, "Microwave photonic image-reject mixer based on a tunable microwave photonic filter with high rejection," *IEEE Photon. J.*, vol. 10, no. 6, Dec. 2018, Art. no. 5502411.
[23] C. B. Albert, C. J. Huang, and E. H. W. Chan, "Brillouin-assisted notch filtering based all-optical image rejection mixer," *IEEE Photon. J.*, vol. 11, no. 2, Apr. 2019, Art. no. 7202712.
[24] Z. Zhu, D.-Y. Choi, S. J. Madden, B. J. Eggleton, and M. Merklein, "High-conversion-gain and deep-image-rejection brillouin chip-based photonic RF mixer," *Opt. Lett.*, vol. 45, no. 19, pp. 5571–5574, Oct. 2020.
[25] X. Xue, X. Zheng, H. Zhang, and B. Zhou, "Widely tunable single-bandpass microwave photonic filter employing a non-sliced broadband optical source," *Opt. Exp.*, vol. 19, no. 19, pp. 18423–18429, Sep. 2011.
[26] C. Yin *et al.*, "Microwave photonic frequency up-convertor with frequency doubling and compensation of chromatic-dispersion-induced power fading," *IEEE Photon. J.*, vol. 9, no. 3, Jun. 2017, Art. no. 5502307.